Asian Journal of Chemistry; Vol. 36, No. 12 (2024), 2848-2854

ASIAN JOURNAL OF CHEMISTRY

https://doi.org/10.14233/ajchem.2024.32718

# Studies of ZnO/NiO/$MoO_3$ Ternary Nanocomposite as an Effective Visible Light Photocatalyst

D. SWAPNA[1,2,*], K. JYOTHI PRIYA[1], V. SRUTHI[1,3], M. SUNETHA[1], R. JAYASHREE[1], G. HIMABINDU[1] and S. PAUL DOUGLAS[1,*]

[1]Department of Engineering Chemistry, AU College of Engineering, Andhra University, Visakhapatnam-530003, India
[2]Department of Chemistry, Dadi Institute of Engineering and Technology, Anakapalli-531002, India
[3]Department of Chemistry, Vignan's Institute of Information and Technology, Duvvada-530049, India

*Corresponding authors: E-mail: dswapna.k@gmail.com; pauldouglas12@gmail.com

*Received*: 16 September 2024; *Accepted*: 25 October 2024; *Published online*: 30 November 2024; AJC-21826

In this work, following a facile coprecipitation technique, a novel ternary ZnO/NiO/$MoO_3$ heterojunction photocatalysts was synthesized and characterized using SEM, TEM, UV-Vis DRS, XRD and FTIR analysis. Under visible light irradiation, the photodegradation of organic pollutants, such as methylene blue, was studied. Comparing the ternary nanocomposite to ZnO, NiO, $MoO_3$ and binary ZnO/NiO, NiO/$MoO_3$ nanocomposite, the former showed better photocatalytic performance. The energy band gap of ZnO/NiO/$MoO_3$ nanocomposite was evaluated using Tauc plot from absorption spectra and resulted as 2.67 eV. The best photocatalytic activity for methylene blue (100%) was shown by ternary ZnO/NiO/$MoO_3$ photocatalyst within 55 min. The development of the ZnO/NiO/$MoO_3$ heterojunction photocatalyst, which is advantageous for effective fast transfer and separation of the photoexcited charge carriers, could be attributed to the better photocatalytic presentation.

**Keywords: ZnO/NiO/$MoO_3$, Ternary nanocomposite, Methylene blue, Photocatalysis.**

## INTRODUCTION

Liquid industrial wastes contain several toxic chemicals, like toxic metals, dyes, pesticides, *etc*. which can cause serious environmental problems. Dye containing discharged wastes are harmful to humans, aquatic life and microbes [1]. As of now, conventional methods such as membrane separation [2], flocculation condensation [3], adsorption [4], oxidation or ozonation [5], reverse osmosis and other techniques have been used to solve such issues. Nevertheless, these techniques are unable to eliminate organic contaminants from water. In recent times, photocatalytic degradation of wastewater has emerged as an encouraging method due to its efficiency, eco-friendliness, environmental compatibility and convenience [6-8]. This comprises of a heterogeneous reaction occurring on the surface of a catalyst, which facilitates the conversion of light energy into the chemical energy. This process includes excitation, redox reactions and recombination, aiming to balance the Fermi energy level of the catalyst with that of the surface adsorbents [9-11].

Because of its photocatalytic activity, metal oxide semiconductors have been seen as a type of promising material to address pollution. Among these, zinc oxide (ZnO), a significant semiconductor material, has drawn a lot of research interest due to its inexpensive nature, superior electrochemical stability and high electron mobility [12,13]. ZnO does, however, also have several defects. It is often active in the presence of UV light and because photoexcited electrons and holes readily recombine, its photocatalytic function is diminished [14,15].

A variety of methods have been used to raise ZnO-based photocatalyst performance [15-30]. Among them is doping with non-metals (C, N, *etc.*) [19,20] or alkali/transition metals [17,18]. Significantly increased photocatalytic activity has been reported for ZnO contained hetero-structures and composites having graphene [21], reduced graphene oxide [22], noble metals [23] and other metal oxides [24-31]. Coupling with p-type oxides is an efficient way to increase the photocatalytic activity of ZnO. Here, the efficiency of photogenerated electron-hole pair separation and the capacity to use light can both be enhanced by the creation of heterojunctions between the n-type ZnO and an appropriate p-type semiconducting oxide. Numerous ZnO binary heterojunctions exist, including ZnO/$MoO_3$ [32], $MoO_3$/ZnO [33] and 1D/1D ZnO@h-$MoO_3$ [34], *etc*. Since, the binary hetero-junctions had higher photo-excited electron hole pair separation and transfer efficiency,

they demonstrated higher photocatalytic activity than single semiconductor materials.

Nickel oxide is a p-type semiconductor known for its non-toxic nature, stability, affordability and wide band gap compared to other semiconductor metal oxides. Additionally, its excellent optical, electrical and photocatalytic properties make it a promising material for photocatalysis applications [35]. Considerable work has gone into changing nickel oxide (NiO) by doping it with non-metals, adding transition metals and combining it with semiconductors in order to increase its photocatalytic activity [36-39]. Previous research demonstrated that enhancing charge separation efficiency and prolonging charge carrier lifetime can improve photocatalytic performance by combining two or more semiconductors with compatible band positions. As a result, merging different semiconductor oxides is considered one of the most effective approaches to achieving high photocatalytic degradation.

Molybdenum trioxide ($MoO_3$), an n-type semiconductor with a well-known band gap of 2.78 eV, is one of the most commonly used materials due to its chemical stability, non-toxic nature and abundant availability. Furthermore, its enhanced dye adsorption capacity plays a key role in photocatalysis [40]. Because of its remarkable capabilities, it has been thought to be an advantageous to develop the Z-scheme heterostructure photocatalyst [41]. According to reports, $MoO_3$ can be joined with other photocatalysts, such as $Bi_2O$ [42], polyimides [43] and CdS [44], to create composites with exceptional photocatalytic activity. This is achieved by lowering charge carrier recombination and enhancing charge transfer processes.

Ternary hetero-junctions demonstrated superior photocatalytic performance compared to binary hetero-junctions in the photodegradation of dyes like phenol, rhodamine B, alizarin yellow, methylene blue and sulfa-methoxazole under visible light irradiation. This enhanced activity is attributed to the rapid separation and transfer of photo excited electron-hole pairs in systems such as $MnO_2/Al_2O_3/Fe_2O_3$ [45], RGO/$TiO_2$/ZnO [46], $MoO_3$/ZnO/$B_2O_3$ [47] and ZnO/$TiO_2$/CdO [48].

However, limited studies have been conducted on ternary hetero-junctions involving molybdenum oxide and zinc oxide based semiconductors. This motivates us to strategically synthesize a ZnO-modified NiO/$MoO_3$ ternary hetero-junction photocatalyst with enhanced photocatalytic performance under sunlight, potentially suitable for everyday applications.

## EXPERIMENTAL

Zinc nitrate hexahydrate ($Zn(NO_3)_2{\cdot}6H_2O$), nickel(II) nitrate hexahydrate ($Ni(NO_3)_2{\cdot}6H_2O$), ammonium molybdate tetrahydrate ($(NH_4)_6Mo_7O_{24}{\cdot}4H_2O$), potassium hydroxide, ethylene glycol, sodium hydroxide, procured from standard companies.

**Synthesis of ZnO:** First, 70 mL of double-distilled water was used to dissolve 0.06 mol of zinc nitrate hexahydrate while stirring constantly at room temperature. Subsequently, 1 mol KOH solution was gradually added to the mixture to keep the solution neutral (pH ~7). The white precipitate was formed after 2 h of stirring the solution at 50 ºC and dried in an oven for 2 h at 100 ºC after being rinsed five times with double-distilled water. To obtain white powder, the dry powder was homogenized with a pestle and mortar. Finally, ZnO nanoparticles were obtained by calcining the white powder for 2 h at 500 ºC in a muffle furnace.

**Synthesis of NiO:** $Ni(NO_3)_2{\cdot}6H_2O$ (0.1 M) dissolved in deionized water was added to a solution containing NaOH (0.8 M) solution dropwise. The mixture was stirred at 80 ºC for 6 h, resulting in the slow formation of a green precipitate. This precipitate was washed several times with double-distilled water and ethanol, then dried at 120 ºC. The obtained NiO nanoparticles were annealed at 600 ºC for 5 h, producing black NiO nanoparticles, which were collected for further study.

**Synthesis of $MoO_3$:** Ethylene glycol (50 mL) were mixed with 250 mL of 0.1 M ammonium molybdate tetrahydrate solution. The mixture was heated for 40 min at 120 ºC, producing a precipitate and a dark blue solution. After centrifugation, the dark blue solution was poured off and the precipitate was washed with distilled water, placed in a dish and placed in the oven at 80 ºC for 24 h. The resultant white molybdenum trioxide powder was treated at different sintering temperatures for 1 h.

For this, 50 mL of ethylene glycol were combined with 250 mL of 0.1 M ammonium molybdate tetrahydrate solution. The mixture was heated at 120 ºC for 40 min, resulting in a precipitate and a dark blue solution. After centrifugation, the dark blue solution was discarded and the precipitate was washed with distilled water, placed in a dish and dried in an oven at 80 ºC for 24 h, yielding white molybdenum trioxide powder. The powder was then annealed at 500 ºC for 1 h.

**Synthesis of ZnO/NiO/$MoO_3$ ternary composites:** ZnO (0.8 g), NiO (0.1 g) and $MoO_3$ (0.1 g) were homogenized together for 1 h to obtain a ternary nanocomposite ZnO/NiO/$MoO_3$.

**Photocatalytic activity:** The photocatalytic performance of ZnO/NiO/$MoO_3$ nanocomposite was evaluated using methylene blue as a model organic dye pollutant. The process was carried out in a visible light photoreactor within an outer wooden cabinet, which was equipped with a magnetic stirrer, a 400 W metal halide lamp, an exhaust fan and an electric power supply. For the reaction, 0.05 g of synthesized ternary nanocomposite was added to 100 mL of 10 ppm methylene blue solution. The suspension was stirred magnetically in the dark for 30 min to establish desorption/absorption equilibrium before exposure to light. During irradiation to the metal halide lamp, samples were collected at regular intervals, centrifuged and the clear dye solution was analyzed for absorbance at 665 nm using a visible spectrophotometer. The photocatalytic activity of the ZnO/NiO/$MoO_3$ nanocomposite was assessed under different conditions, including varying pH levels (2-10), irradiation times (5-140 min), methylene blue concentrations (5-100 ppm) and photocatalyst dosages (0.2-1 g/L).

**Characterization:** Brucker DX-5 X-ray diffraction (XRD) was used for the phase and crystalline structure at $\lambda = 1.54$ Å with $2\theta$ ranging from 10-90º. IR Prestige 21 was used to record FTIR spectra in the 4000-500 $cm^{-1}$ range. With the use of field emission scanning electron microscopy (Carl Zeiss, Germany), the size and shape of the particles were examined. High resolution transmission electron microscope (model: Zeiss Gemini 300). The 2600R Shimadzu was used to measure the optical

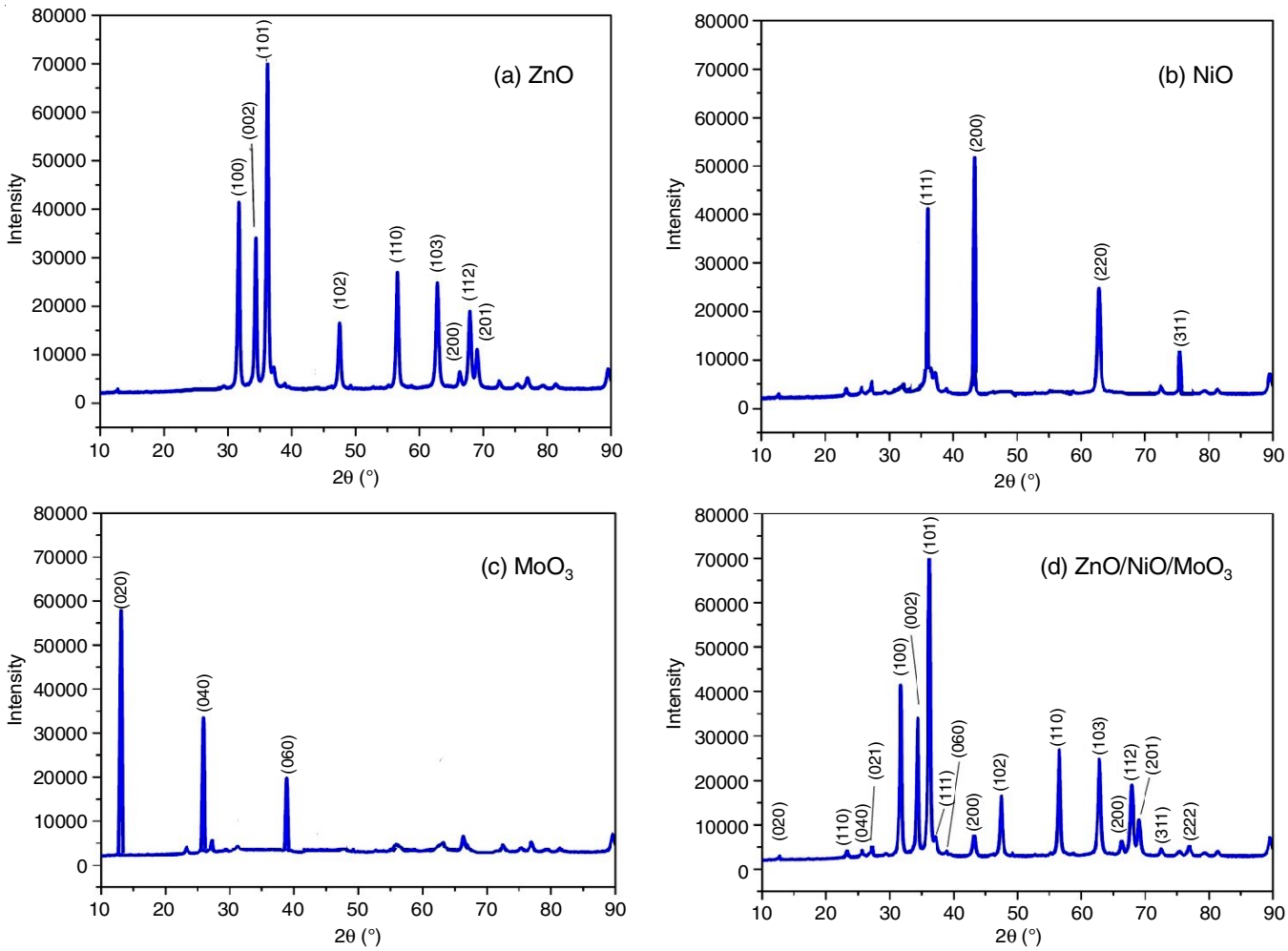


Fig. 1. XRD patterns of the ZnO, NiO, $MoO_3$ and ZnO/NiO/$MoO_3$ nanocomposite

band gap UV-vis DRS, with $BaSO_4$ serving as the reference wavelength, spanning from 200 to 800 nm.

## RESULTS AND DISCUSSION

**X-ray diffraction studies:** The different ratios of ZnO, NiO and $MoO_3$ were combined to obtain homogenous ternary composites. Fig. 1d shows the XRD spectrum of ZnO/NiO/$MoO_3$ nanocomposite. The diffraction peaks for $MoO_3$ were in accordance with JCPDS No.05-0508. the main characteristic peaks located in 2θ = 12.80º, 25.70º and 39.00º are indexed to (020), (040) and (060) crystal planes. NiO exhibits four different peaks at about 2θ = 37.20º, 43.30º, 62.90º and 75.50º correspond to the crystal plane (111), (200), (220) and (311) (JCPDS card No.47-1049). ZnO observed diffraction peaks (100), (002), (101), (102), (110), (103), (200), (112) and (201) well matched with JCPDS card no. 89-0510.

**FTIR studies:** The FTIR spectrum of ZnO/NiO/$MoO_3$ heterojunctions in the 4000-400 $cm^{-1}$ region is shown in Fig. 2. The bonds between inorganic elements are typically the cause of band frequencies that occur below 800 $cm^{-1}$. The stretching vibration of the Zn-O bond in tetrahedral and octahedral coordination is responsible for the significant bands observed at 500 and 600 $cm^{-1}$, respectively.

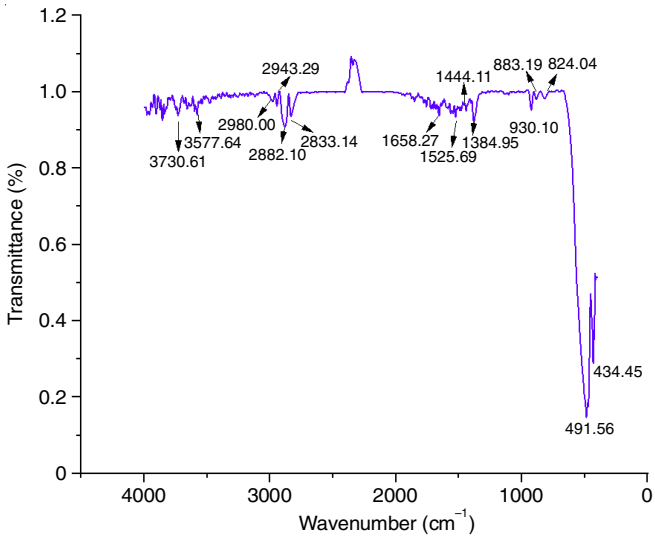


Fig. 2. FTIR spectrum of ZnO/NiO/$MoO_3$ nanocomposite

The nanocomposite's molecular interaction is observed at 434.45, 491.56, 1000-800, 1700-1300, 3000-2800 and 3800-3500 $cm^{-1}$. The Ni-O stretching is represented by the strong band at 434.45 $cm^{-1}$, the Zn-O stretching by 491.56 $cm^{-1}$ and the $MoO_3$ absorption peaks range from 820 to 935 $cm^{-1}$. The

H-O-H bending, 3577.64 $cm^{-1}$ O-H stretching bond, is indicated by the peak ~1525.69 $cm^{-1}$.

**UV-DRS studies:** Fig. 3 shows the ZnO/NiO/$MoO_3$ UV-visible absorption spectrum. The maximum absorption peak is within the visible range. Using Tauc's relation, the optical bandgap of the ZnO/NiO/$MoO_3$ nanocomposite was calculated using $(\alpha h\nu)^2 = A(h\nu - E_g)$, where ν is the photon energy (eV), h is Planck's constant, α is the coefficient of absorption and $E_g$ is the bandgap energy (eV). The bandgap energy can be calculated by plotting the $(\alpha h\nu)^2$ *versus* hν as shown in Fig. 3 and extrapolating the line drawn tangent to the resulting curve. The bandgap of the ZnO/NiO/$MoO_3$ nanocomposite was found to be 2.67 eV.

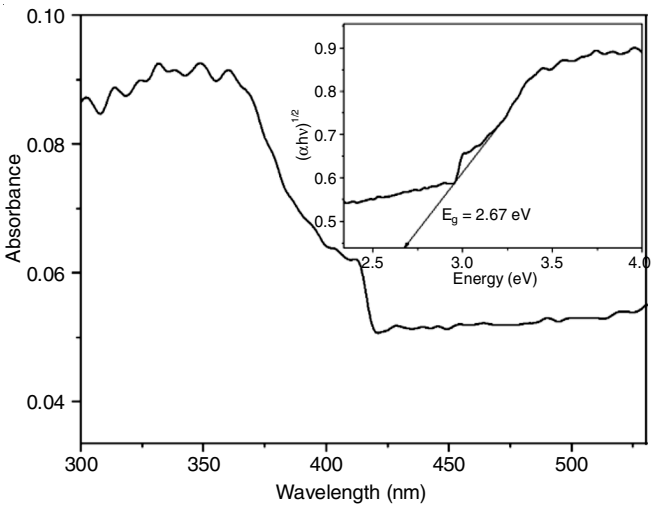


Fig. 3. Diffuse reflectance spectrum of ZnO/NiO/$MoO_3$ nanocomposite (Inset shows the Tauc plot of ZnO/NiO/$MoO_3$ nanocomposite)

**FE-SEM studies:** Fig. 4a-b reveals that the nano composite is spherical in shape and exhibit a generally uniform size. SEM analysis indicated that the average particle size of the samples was 35.69 nm.

**EDX studies:** Fig. 5 displays the typical EDX spectra of the ZnO/NiO/$MoO_3$ nanocomposite. The elements Zn, Ni, Mo and O were present in amounts of 57.31, 3.25, 6.66 and 32.78, respectively. Furthermore, no extra peaks were observed that corresponded to any other elements.

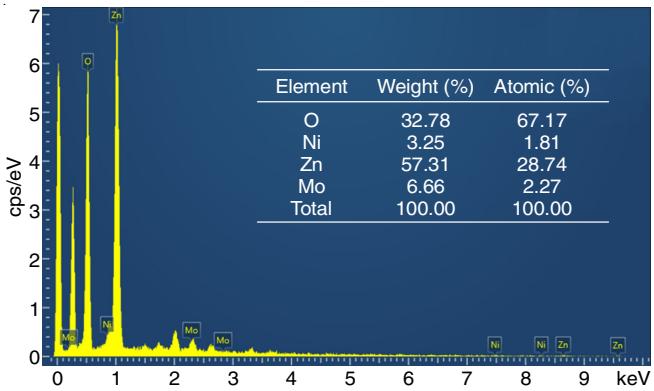


Fig. 5. EDX Spectra of ZnO/NiO/$MoO_3$ nanocomposite

**TEM studies:** The HR-TEM images were captured by dispersing ZnO/NiO/$MoO_3$ nanocomposite in ethanol on a carbon coated copper grid. The HR-TEM image (Fig. 6) clearly shows that the ZnO particles are polycrystalline and exhibit a spherical shape with agglomeration.

**Photocatalytic activity:** Methylene blue was employed in a photocatalytic degradation experiment. The photocatalytic performance of the nanocomposite was evaluated under varying conditions, including pH, irradiation time, methylene blue concentration and photocatalyst dose. To determine the optimal conditions, parameter optimization studies were conducted for pH, dye concentration, catalyst amount and irradiation.

**Effect of dye concentration:** To assess the effect of dye concentration on the degradation efficiency of the synthesized photocatalyst, methylene blue concentrations were varied from 5 to 100 ppm and irradiation times were set up to 140 min. The rate of degradation is influenced by the production of radicals by the photocatalyst and their interactions with the dye molecules. At higher dye concentrations, the dye ions can shield the active sites of the photocatalyst, reducing the formation of hydroxyl radicals (•OH) on the surface of catalyst. Moreover, a higher concentration of dye molecules can absorb a significant amount of visible light, which decreases the radiation level [35]. As shown in Fig. 7, the removal of methylene blue dye was most effective at a lower concentration of 10 ppm for the catalyst.

**Effect of pH:** The pH of the solution is a crucial factor in photdegradation processes, as it significantly influences the

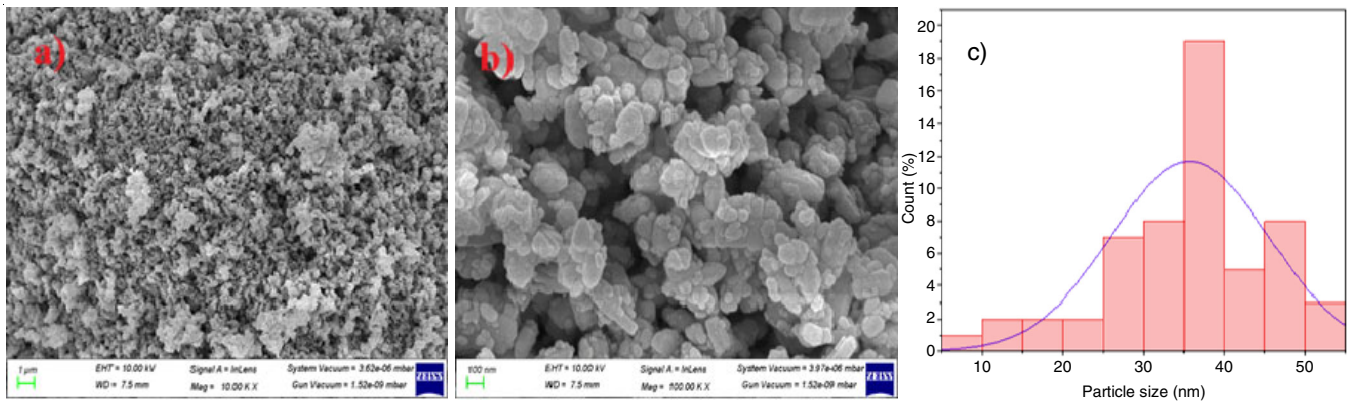


Fig. 4. SEM images of ZnO/NiO/$MoO_3$ (a) 1 μm (b) 100 nm (c) particle size distribution of ZnO/NiO/$MoO_3$ nanocomposite

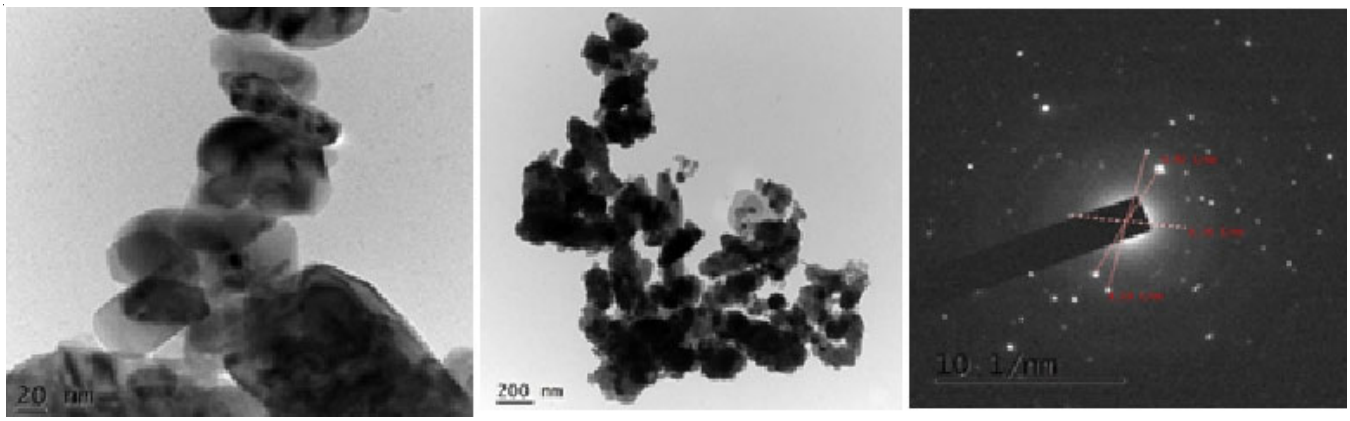


Fig. 6. TEM images of ZnO/NiO/$MoO_3$ nanocomposite

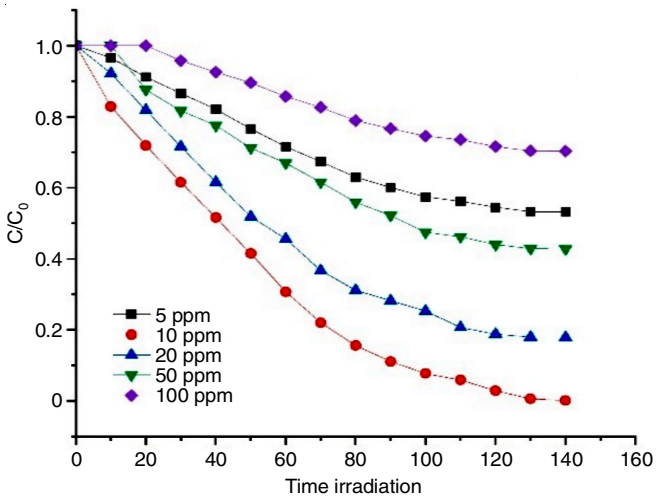


Fig. 7. Effect of methylene blue concentration on photodegradation

surface charge of the photocatalyst. Fig. 8 illustrates the effect of solution pH on the rate of photocatalytic degradation using ZnO/NiO/$MoO_3$ over a pH range from 2 to 10. The results show that increasing the pH from 2 to 8 enhances the rate of photocatalytic degradation methylene blue. However, the degradation process levels off when the pH exceeds 8. Based on these findings, a pH of 8 was identified as the optimal condition.

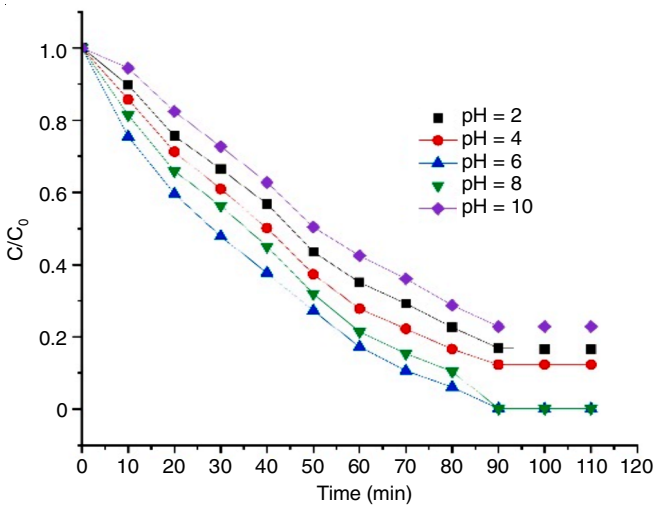


Fig. 8. Effect of pH on degradation of methylene blue

**Effect of temperature:** Temperature variations have a significant impact on the photodegradation process. This is according to the findings, which demonstrate that temperature increases the rate of disintegration. The influence of temperature on visible light is shown in Fig. 9, which illustrated that the optimum rate of degradation occurs at 35 ºC.

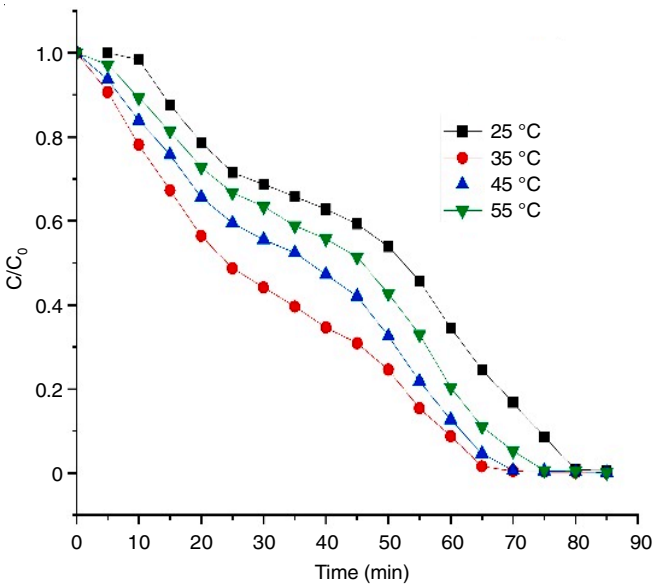


Fig. 9. Effect of temperature on photodegradation of methylene blue

**Effect of photocatalyst amount:** The effect of photocatalyst quantity on methylene blue removal was investigated by varying the amount from 0.2 to 1 g in 0.2 g increments, while keeping other optimized conditions (pH 8, 10 ppm methylene blue solution and 35 ºC). Fig. 10 shows that the degradation efficiency of methylene blue molecules increases with photocatalyst amounts up to 0.4 g/L; beyond this concentration, the efficiency decreases. An increase in the photocatalyst concentration enhances the proliferation of superoxide and hydroxyl radicals due to more active sites at the molecular level. However, excessive photocatalyst concentration can lead to coagulation of catalyst nanoparticles, reducing surface area and photon absorption, which in turn decreases the rate of photocatalytic degradation [49]. Based on these results, 0.4 g/L was found to be the optimal photocatalyst concentration.

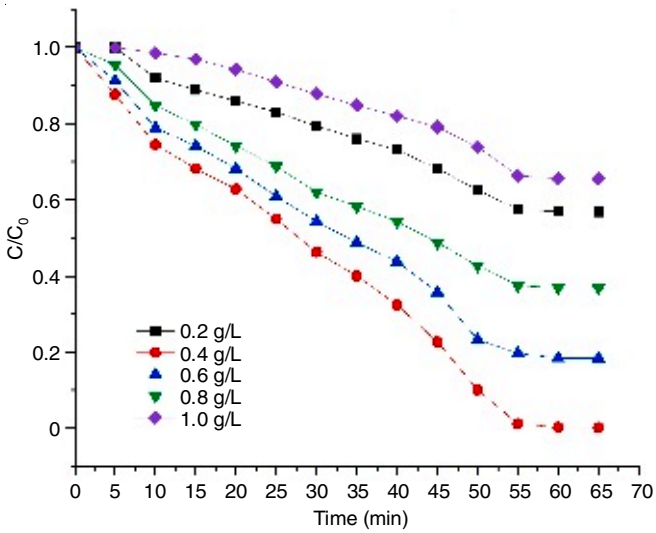


Fig. 10. Effect of catalyst amount on the photodegradation of methylene blue

**Effect of irradiation time:** Another factor that influences the photocatalytic efficiency of ZnO, NiO, $MoO_3$ and ZnO/NiO/$MoO_3$ nanocatalyst in the elimination of methylene blue is the time period of irradiation. The irradiation time was changed from 5 to 65 min while the optimized was conducted at pH 8, 10 ppm of methylene blue solution and temperature 35 ºC, which was the optimal setting. From Fig. 11, up to 55 min of irradiation, the prepared photocatalyst for methylene blue showed an increase in degrading efficiency; beyond that the value remained constant. The optimum irradiation time was found to be 55 min.

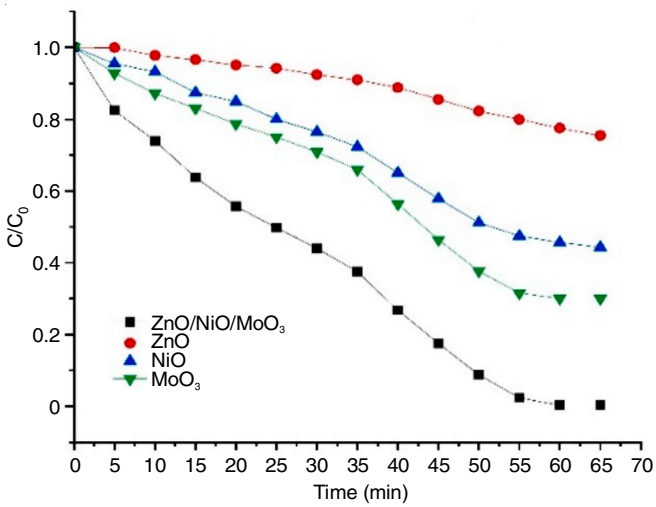


Fig. 11. Effect of irradiation time on photodegradation of methylene blue

**Recyclability test:** After the methylene blue degradation, the catalyst was collected for the recyclability test. The ZnO/NiO/$MoO_3$ nanocomposite was examined and three cycles of methylene blue degradation under optimal conditions were studied. As more cycles are added, the ZnO/NiO/$MoO_3$ composite shows a progressive decline in catalytic efficiency. The recyclability of ZnO/NiO/$MoO_3$ nanocomposite were well organized up to three cycles (Fig. 12).

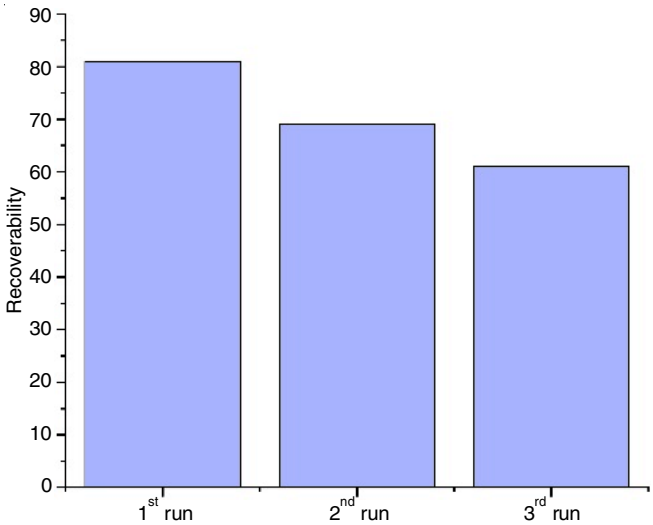


Fig. 12. Degradation effiency of methylene blue under three different cycles

## Conclusion

The coprecipitation approach was used to develop ternary ZnO/NiO/$MoO_3$ nanocomposites as well as pure ZnO, NiO and $MoO_3$ nanoparticles. Under visible irradiation, the photocatalytic degradation of methylene blue using ternary nanocomposite ZnO/NiO/$MoO_3$ was found to be very efficient and acheived within 55 min. The XRD results showed no appearance of secondary phases in the ternary nanocomposite. In terms of reusability assessments, the ternary nanocomposite maintained its activity upto three cycles only, preserving over 62% of its initial degradation efficiency.

## ACKNOWLEDGEMENTS

The authors thank Advanced Analytical Laboratory, Andhra University, Visakhapatnam, India for providing the spectral analysis.

## CONFLICT OF INTEREST

The authors declare that there is no conflict of interests regarding the publication of this article.

## REFERENCES

1. P. Borker and A.V. Salker, *Mater. Sci. Eng. B*, **133**, 55 (2006); https://doi.org/10.1016/j.mseb.2006.05.007
2. J. Dasgupta, J. Sikder, S. Chakraborty, S. Curcio and E. Drioli, *J. Environ. Manage.*, **147**, 55 (2015); https://doi.org/10.1016/j.jenvman.2014.08.008
3. X.M. Tang, H.L. Zheng, H.K. Teng, Y.J. Sun, J.S. Guo, W.Y. Xie, Q.Q. Yang and W. Chen, *Desalination Water Treat.*, **57**, 1733 (2016); https://doi.org/10.1080/19443994.2014.977959
4. R. Gusain, K. Gupta, P. Joshi and O. Khatri, *Adv. Colloid Interface Sci.*, **272**, 102009 (2019); https://doi.org/10.1016/j.cis.2019.102009
5. E.L. Hu, S.M. Shang, X.M. Tao, S.X. Jiang and K.L. Chiu, *J. Clean. Prod.*, **137**, 1055 (2016); https://doi.org/10.1016/j.jclepro.2016.07.194
6. P.A.K. Reddy, P.V.L. Reddy, E. Kwon, K.H. Kim, T. Akter and S. Kalagara, *Environ. Int.*, **91**, 94 (2016); https://doi.org/10.1016/j.envint.2016.02.012

7. N. Yahya, F. Aziz, N.A. Jamaludin, M. A. Mutalib, A.F. Ismail, W.N. W. Salleh, J. Jaafar, N. Yusof and N. A. Ludin, *J. Environ. Chem. Eng.*, **6**, 7411 (2018); https://doi.org/10.1016/j.jece.2018.06.051
8. B.S. Liu, X.J. Zhao, C. Terashima, A. Fujishima and K. Nakata, *Phys. Chem. Chem. Phys.*, **16**, 8751 (2014); https://doi.org/10.1039/c3cp55317e
9. V. Augugliaro, M. Litter, L. Palmisano and J. Soria, *J. Photochem. Photobiol. Photochem. Rev.*, **7**, 127 (2006); https://doi.org/10.1016/j.jphotochemrev.2006.12.001
10. J.M. Herrmann, *Appl. Catal. B*, **99**, 461 (2010); https://doi.org/10.1016/j.apcatb.2010.05.012
11. C.B. Ong, L.Y. Ng and A.W. Mohammad, *Renew. Sustain. Energy Rev.*, **81**, 536 (2018); https://doi.org/10.1016/j.rser.2017.08.020
12. F.X. Wang, L. Liang, L. Shi, M.S. Liu and J.M. Sun, *Dalton Trans.*, **43**, 16441 (2014); https://doi.org/10.1039/C4DT02098G
13. C.C. Hu, L. Lu, Y.J. Zhu, R. Li and Y.J. Xing, *Mater. Chem. Phys.*, **217**, 182 (2018); https://doi.org/10.1016/j.matchemphys.2018.06.068
14. J.H. Lang, J.Y. Wang, Q. Zhang, X.Y. Li, Q. Han, M.B. Wei, Y.R. Sui, D.D. Wang and J.H. Yang, *Ceram. Int.*, **42**, 14175 (2016); https://doi.org/10.1016/j.ceramint.2016.06.042
15. A. Samanta, M.N. Goswami and P.K. Mahapatra, *Physica E*, **104**, 254 (2018); https://doi.org/10.1016/j.physe.2018.07.042
16. Z. Zhang, G. Chen and D.W. Bahnemann, *J. Mater. Chem.*, **19**, 5089 (2009); https://doi.org/10.1039/b821991e
17. H. Benhebal, M. Chaib, A.L. Leonard, S.D. Lambert and M. Crine, *Mater. Sci. Semicond. Process.*, **15**, 264 (2012); https://doi.org/10.1016/j.mssp.2011.12.001
18. R. Saleh and N.F. Djaja, *Spectrochim. Acta A Mol. Biomol. Spectrosc.*, **130**, 581 (2014); https://doi.org/10.1016/j.saa.2014.03.089
19. S.A. Ansari, S. Ansari, H. Foaud and M. Cho, *New J. Chem.*, **41**, 9314 (2017); https://doi.org/10.1039/C6NJ04070E
20. R. Rangel, V. Cedeño, A. Ramos-Corona, R. Gutiérrez, J.J. Alvarado-Gil, O. Ares, P. Bartolo-Pérez and P. Quintana, *Appl. Phys*., *A Mater. Sci. Process.*, **123**, 552 (2017); https://doi.org/10.1007/s00339-017-1137-5
21. B. Xue and Y. Zou, *Appl. Surf. Sci.*, **440**, 1123 (2018); https://doi.org/10.1016/j.apsusc.2018.01.299
22. J. Qin, X. Zhang, C. Yang, M. Cao, M. Ma and R. Liu, *Appl. Surf. Sci.*, **392**, 196 (2017); https://doi.org/10.1016/j.apsusc.2016.09.043
23. R. Raji, K.S. Sibi and K.G. Gopchandran, *Appl. Surf. Sci.*, **427**, 863 (2018); https://doi.org/10.1016/j.apsusc.2017.09.050
24. Z. Zhang, C. Shao, X. Li, C. Wang, M. Zhang and Y. Liu, *ACS Appl. Mater. Interfaces*, **2**, 2915 (2010); https://doi.org/10.1021/am100618h
25. P. Shukla and J.K. Shukla, *J. Sci. Adv. Mater. Devices*, **3**, 452 (2018); https://doi.org/10.1016/j.jsamd.2018.09.005
26. C. Luo, D. Li, W. Wu, Y. Zhang and C. Pan, *RSC Adv.*, **4**, 3090 (2014); https://doi.org/10.1039/C3RA44670K
27. Y. Liu, G. Li, R. Mi, C. Deng and P. Gao, *Sens. Actuators B Chem.*, **191**, 537 (2014); https://doi.org/10.1016/j.snb.2013.10.068
28. M. Xiao, Y. Lu, Y. Li, H. Song, L. Zhu and Z. Ye, *RSC Adv.*, **4**, 34649 (2014); https://doi.org/10.1039/C4RA04600E
29. B. Li and Y. Wang, *Superlattices Microstruct.*, **47**, 615 (2010); https://doi.org/10.1016/j.spmi.2010.02.005
30. R.K. Sharma, D. Kumar and R. Ghose, *Ceram. Int.*, **42**, 4090 (2016); https://doi.org/10.1016/j.ceramint.2015.11.081
31. K.H. Kim, Y. Yoshihara, Y. Abe, M. Kawamura and T. Kiba, *Mater. Lett.*, **186**, 364 (2017); https://doi.org/10.1016/j.matlet.2016.10.052
32. J. Huang, X. Wang, S. Li and Y. Wang, *Appl. Surf. Sci.*, **257**, 116 (2010); https://doi.org/10.1016/j.apsusc.2010.06.046
33. M. Tanveer, I. Nisa, G. Nabi, M. Khalid Hussain, S. Khalid and M.A. Qadeer, *J. Magn. Magn. Mater.*, **553**, 169245 (2022); https://doi.org/10.1016/j.jmmm.2022.169245
34. D. Saminathan, T. Deogratias, S. Thirugnanasambandan, N. Vengidusamy and S. Arumainathan, *Mater. Lett.*, **262**, 127049 (2020); https://doi.org/10.1016/j.matlet.2019.127049
35. C. Han, R. Zhang, Y. Ye, L. Wang, Z. Ma, F. Su, H. Xie, Y. Zhou, P.K. Wong and L. Ye, *J. Mater. Chem. A Mater. Energy Sustain.*, **7**, 9726 (2019); https://doi.org/10.1039/C9TA01061K
36. A.K. Ramasami, M.V. Reddy and G.R. Balakrishna, *Mater. Sci. Semicond. Process.*, **40**, 194 (2015); https://doi.org/10.1016/j.mssp.2015.06.017
37. S. Sankar, S.K. Sharma, N. An, H. Lee, D.Y. Kim, Y.B. Im, Y.D. Cho, R.S. Ganesh, S. Ponnusamy, P. Raji and L.P. Purohit, *Optik*, **127**, 10727 (2016); https://doi.org/10.1016/j.ijleo.2016.08.126
38. D.D. Joyal Mary, V. Baiju, R. Biju and R. Raveendran, *Int. J. Adv. Res. Sci. Eng*, **06**, 284 (2017).
39. A. Khatri and P. Rana, *Bull. Mater. Sci.*, **42**, 141 (2019); https://doi.org/10.1007/s12034-019-1835-z
40. B. Feng, Z. Wu, J. Liu, K. Zhu, Z. Li, X. Jin, Y. Hou, Q. Xi, M. Cong, P. Liu and Q. Gu, *Appl. Catal. B*, **206**, 242 (2017); https://doi.org/10.1016/j.apcatb.2017.01.029
41. L. Huang, H. Xu, R. Zhang, X. Cheng, J. Xia, Y. Xu and H. Li, *Appl. Surf. Sci.*, **283**, 25 (2013); https://doi.org/10.1016/j.apsusc.2013.05.106
42. Z. Hu, J. Zhou, Y. Zhang, W. Liu, J. Zhou and W. Cai, *Chem. Phys. Lett.*, **706**, 208 (2018); https://doi.org/10.1016/j.cplett.2018.06.006
43. C. Ma, J. Zhou, H. Zhu, W. Yang, J. Liu, Y. Wang and Z. Zou, *ACS Appl. Mater. Interfaces*, **7**, 14628 (2015); https://doi.org/10.1021/acsami.5b01356
44. Z. Xie, Y. Feng, F. Wang, D. Chen, Q. Zhang, Y. Zeng, W. Lv and G. Liu, *Appl. Catal. B*, **229**, 96 (2018); https://doi.org/10.1016/j.apcatb.2018.02.011
45. H.L. Haile, T. Abi and K. Tesfahun, *Afr. J. Pure Appl. Chem.*, **9**, 211 (2015); https://doi.org/10.5897/AJPAC2015.0656
46. F.T. Johra and W.G. Jung, *Appl. Catal. A Gen.*, **491**, 52 (2015); https://doi.org/10.1016/j.apcata.2014.11.036
47. M. Fabian, E. Svab and K. Krezhov, *J. Non-Cryst. Solids*, **433**, 6 (2016); https://doi.org/10.1016/j.jnoncrysol.2015.11.023
48. G.K. Upadhyay, J.K. Rajput, T.K. Pathak, P.K. Pal and L.P. Purohit, *Appl. Surf. Sci.*, **509**, 145326 (2020); https://doi.org/10.1016/j.apsusc.2020.145326
49. S. Sharma, R. Sharma and A.K. Sharma, *Curr. Environ. Eng.*, **5**, 221 (2018); https://doi.org/10.2174/2212717805666180801143324